

Probing the atmosphere of the bulge G5III star OGLE-2002-BUL-069 by analysis of microlensed $H\alpha$ line *

A. Cassan^{1,2}, J.P. Beaulieu^{1,2}, S. Brillant^{1,3}, C. Coutures^{1,2,4}, M. Dominik^{1,5}, J. Donatowicz^{1,6}, U.G. Jørgensen^{1,7},
D. Kubas^{1,8}, M.D. Albrow^{1,9}, J.A.R. Caldwell^{1,10}, P. Fouqué^{1,11}, J. Greenhill^{1,12}, K. Hill^{1,12}, K. Horne^{1,5},
S. Kane^{1,5}, R. Martin^{1,13}, J. Menzies^{1,14}, K.R. Pollard^{1,9}, K.C. Sahu^{1,10}, C. Vinter⁷, J. Wambsganss^{1,8},
R. Watson^{1,12}, A. Williams^{1,13}, C. Fendt⁸, P. Hauschildt¹⁵, J. Heinmueller⁸, J. B. Marquette², and C. Thurl¹⁶

¹ PLANET collaboration member

² Institut d’Astrophysique de Paris, 98bis Boulevard Arago, 75014 Paris, France

³ European Southern Observatory, Casilla 19001, Vitacura 19, Santiago, Chile

⁴ DSM/DAPNIA, CEA Saclay, 91191 Gif-sur-Yvette cedex, France

⁵ University of St Andrews, School of Physics & Astronomy, North Haugh, St Andrews, KY16 9SS, United Kingdom

⁶ Technical University of Vienna, Dept. of Computing, Wiedner Hauptstrasse 10, Vienna, Austria

⁷ Niels Bohr Institute, Astronomical Observatory, Juliane Maries Vej 30, DK-2100 Copenhagen, Denmark

⁸ Universität Potsdam, Astrophysik, Am Neuen Palais 10, D-14469 Potsdam, Germany

⁹ University of Canterbury, Department of Physics & Astronomy, Private Bag 4800, Christchurch, New Zealand

¹⁰ Space Telescope Science Institute, 3700 San Martin Drive, Baltimore, MD 21218, USA

¹¹ Observatoire Midi-Pyrenees, UMR 5572, 14, avenue Edouard Belin, F-31400 Toulouse, France

¹² University of Tasmania, Physics Department, GPO 252C, Hobart, Tasmania 7001, Australia

¹³ Perth Observatory, Walnut Road, Bickley, Perth 6076, Australia

¹⁴ South African Astronomical Observatory, P.O. Box 9 Observatory 7935, South Africa

¹⁵ Hamburger Sternwarte, Gojenbergsweg 112, 21029 Hamburg, Germany

¹⁶ RSAA, Mount Stromlo and Siding Spring Observatories, ANU, Cotter Road, Weston Creek, Canberra, ACT 2611, Australia

Received ; accepted

Abstract. We discuss high-resolution, time-resolved spectra of the caustic exit of the binary microlensing event OGLE 2002-BLG-069 obtained with UVES on the VLT. The source star is a G5III giant in the Galactic Bulge. During such events, the source star is highly magnified, and a strong differential magnification around the caustic resolves its surface. Using an appropriate model stellar atmosphere generated by the PHOENIX v2.6 code we obtain a model light curve for the caustic exit and compare it with a dense set of photometric observations obtained by the PLANET microlensing follow up network. We further compare predicted variations in the $H\alpha$ equivalent width with those measured from our spectra. While the model and observations agree in the gross features, there are discrepancies suggesting shortcomings in the model, particularly for the $H\alpha$ line core, where we have detected amplified emission from the stellar chromosphere after the source star’s trailing limb exited the caustic. This achievement became possible by the provision of the very efficient OGLE-III Early Warning System, a network of small telescopes capable of nearly-continuous round-the-clock photometric monitoring, on-line data reduction, daily near-real-time modelling in order to predict caustic crossing parameters, and a fast and efficient response of a 8m class telescope to a “Target-Of-Opportunity” observation request.

Key words. Techniques: gravitational microlensing – Techniques: high resolution spectra – Techniques: high angular resolution – Stars: atmosphere models – Stars: individual (OGLE 2002-BLG-069)

1. Introduction

Near extended caustics produced by binary (or multiple) lenses, the source star undergoes a large total magnification in brightness. Furthermore, its surface is differentially magnified be-

cause of a strong gradient in magnification. The relative lens-source proper motion is typically slow enough to allow the light curve to be frequently sampled. This translates to a high spatial resolution on the source star’s surface and hence permits its radial brightness profile to be inferred from the observations. Over the past four years, coefficients characterizing linear or square-root limb-darkening profiles have been obtained with the microlensing technique for several Bulge giants and sub-

Send offprint requests to: beaulieu@iap.fr

* Based on observations made at ESO, 69.D-0261(A), 269.D-5042(A), 169.C-0510(A)

giants (Fields et al. 2003 and references therein) and a main sequence star (Abe et al. 2003). A new generation of stellar atmosphere models (Orosz & Hauschildt 2000) have revealed limb-darkening laws that are significantly different from the traditional analytic ones (Bryce et al. 2002; Claret & Hauschildt 2003). The centre to limb variation of spectral lines can show markedly different behaviour from that of the continuum. Most moderately strong and weak lines weaken towards the limb, but resonant scattering lines can vary in a much more pronounced way (Loeb & Sasselov 1995). In cool giants, $H\beta$, being formed lower in the atmosphere, is more limb-darkened than $H\alpha$. TiO and Ca II show strong variations, and some lines and bands may even be limb-brightened. Intensive spectroscopic monitoring of a caustic exit at high resolution with high S/N should reveal temporal variations in the equivalent widths of promising spectral lines that can be compared with predictions from stellar atmosphere models (Heyrovský et al. 2000).

We present here the first photometric and spectroscopic monitoring campaign that has successfully been performed at high resolution with dense sampling. Previously, Castro et al. (2001) obtained two KECK HIRES spectra of EROS 2000-BLG-5, but missed the trailing limb of the caustic where the effects are stronger, while the data in the qualitative analysis of Albrow et al. (2001) involved dense coverage but at low resolution. Afonso et al. (2001) provided a model that reproduces the photometric data and found an excess of $H\alpha$ at the limb. They attribute the excess to chromospheric emission, but it could be due to shortcomings of the synthetic spectra. Using a determination of the spectral type of the source star, we have computed the limb-darkening profiles in R and I from appropriate PHOENIX synthetic spectra of the source star and fitted a fold-caustic model to our photometric data obtained during the caustic exit. This model has been used here to compute the synthetic spectrum for wavelengths around the $H\alpha$ -line. A more detailed report on the determination of the stellar parameters and the analysis of other spectral lines will be presented elsewhere (Beaulieu et al. 2004), as will the details of a full binary lens model fit to the PLANET observations of the event (Kubas et al. 2004).

2. OGLE 2002-BLG-069 photometry and spectroscopy

The PLANET collaboration, comprising six different telescopes, namely, SAAO 1.0m (South Africa), Danish 1.54m (Chile), ESO 2.2m (Chile), Canopus 1.0m (Australia), Mt. Stromlo 50in (Australia) and Perth 0.6m (Australia), commenced photometric observations of OGLE 2002-BLG-069 alerted by the OGLE-III early Warning System (Udalski 2003) in early June, 2002. From online data reductions on 25 June it was realised that the event involved a binary lens and a bright giant source star. With the source taking ~ 1.4 days to cross the caustic on entry, it appeared to be an excellent candidate for time-resolved spectroscopy of the caustic exit. Using the predictions based on modeling our photometry, and thanks to excellent coordination with the staff at La Silla and Paranal, very good coverage was obtained during the caustic exit together with post-caustic reference spectra. These obser-

vations were performed using the UVES spectrograph mounted on Kueyen (VLT UT2) as part of Target-of-Opportunity and Director’s Discretionary time. Thirty-nine spectra with exposure time of 20 min (1 hour for the post caustic observations) were obtained alternately in the so-called standard settings, 580 and 860, covering the full 4800 – 10600 Å range at a resolution of 30000 with S/N ranging from 50 to 130. From an analysis of the curve-of-growth of 100 Fe I and Fe II lines as done by Minniti et al. (2002), and independently from the study of the Ca II and Mg lines (Jørgensen et al. 1992), a good fit to all the data was obtained with a plane-parallel model atmosphere having $T_{\text{eff}} = 5000$ K, $\log(g) = 2.5$, $v_{\text{turb}} = 1.5 \text{ km s}^{-1}$ and $[\text{Fe}/\text{H}] = -0.6$. The calibration of the MK spectral type gives, for a G5III star, $T_{\text{eff}} = 5050$ K, $M_V = +0.9$, $(V - I) = 0.95$, $M/M_{\odot} = 1.1$ and $R/R_{\odot} = 10$. At HJD=2452455.2754, the source was amplified by 17.7. The measured color from SAAO data are $I = 13.01 \pm 0.01$, $(V - I) = 2.06 \pm 0.02$, so $E(V - I) = 1.11 \pm 0.02$. We adopt a conservative $A_V/E(V - I) = 2.2 \pm 0.3$, and then derive a distance of 9.4 ± 1.4 kpc.

3. Modeling of the caustic exit

With ρ denoting the fractional radius of the source star, we approximate its wavelength-dependent brightness profile $I^{\lambda}(\rho) = \bar{I}\xi^{\lambda}(\rho)$ by concentric rings of constant intensity. A model atmosphere for the stellar parameters given in the previous section was computed with the PHOENIX grid v2.6 (based on the code described by Allard et al. (2001) but using spherical geometry and spherically symmetric radiative transfer). A synthetic spectrum was calculated from this model at a spectral resolution of 0.05 Å at 128 steps in source radius. The intensity profile was interpolated with cubic splines at 1000 points equally spaced in $\cos \vartheta = \sqrt{1 - \rho^2}$ where ϑ is the emergent angle, so that the width of the rings of constant intensity decreases toward the stellar limb. For a broadband filter (s), the intensity profile $\xi^{(s)}(\rho)$ is obtained by convolving the source brightness profile with the filter, CCD transmission and atmosphere response functions. The observed magnitude $m^{(s)}(t)$ reads $m^{(s)}(t) = m_S^{(s)} - 2.5 \lg \{A^{(s)}(t) + g^{(s)}\}$ where $m_S^{(s)}$ is the intrinsic source magnitude, $g^{(s)} = F_B^{(s)}/F_S^{(s)}$ is the ratio between background flux $F_B^{(s)}$ and intrinsic source flux $F_S^{(s)}$, and $A^{(s)}(t)$ the source magnification at time t .

The photometric data presented in the lower panel of Fig. 1 show a peak with the characteristic shape resulting from a fold-caustic exit. For a source in the vicinity of a fold caustic, the magnification $A^{(s)}(t)$ can be decomposed (e.g., Albrow et al. 1999a) as $A^{(s)}(t) = A_{\text{crit}}^{(s)}(t) + A_{\text{other}}(t)$, where $A_{\text{crit}}^{(s)}(t)$ denotes the magnification of the critical images associated with the caustic, and $A_{\text{other}}(t)$ denotes the magnification of the remaining images of the source under the action of the binary lens.

Let us consider a uniformly moving source crossing the caustic within $2\Delta t$ and exiting the caustic by its trailing limb at t_f . If one neglects the curvature of the caustic and the variation of its strength over the size of the source, the magnification of the critical images reads $A_{\text{crit}}^{(s)}(t) =$

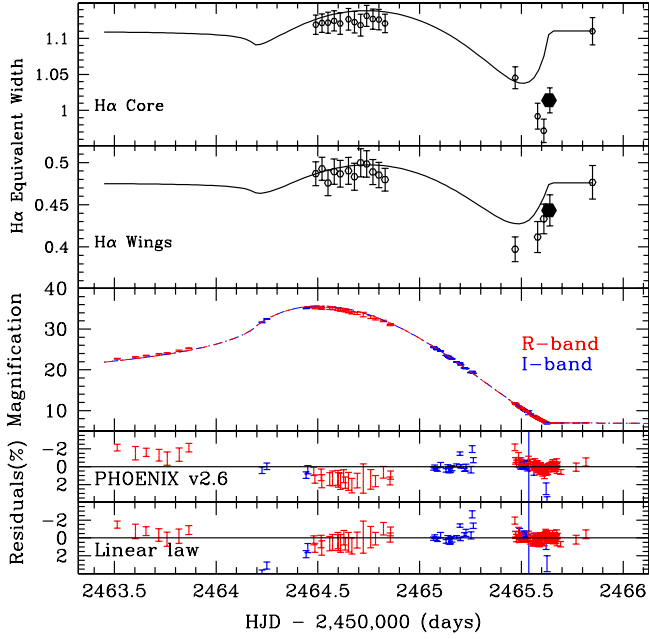


Fig. 1. Equivalent-width variation of the H α core (top panel) and wings (second panel from the top); the open circles in the plots of the equivalent-width variation correspond to our UVES data, while the adjoining solid lines represent the model predictions over the course of the caustic passage. The big dots correspond to the spectra of 10 July, UT 02H58. Third panel: model light curves and photometric data, where R-band data are plotted in red and I-band data in blue; model residuals from the chosen PHOENIX atmosphere (fourth panel) and from the linear limb-darkening law (bottom panel), with the same color convention. The model parameters can be found in Tab. 1. The majority of model residuals are below the 2 % level. The post caustic observations have been plotted at 2465.85, but have been taken on 16 August.

$a_{\text{crit}} G_f\left(-\frac{t-t_f}{\Delta t}; \xi^{(s)}\right)$ where $G_f(\eta; \xi^{(s)})$ is a characteristic function (Schneider & Wagoner 1987) which solely depends on the intensity profile $\xi^{(s)}$. For $|\omega(t - t_f)| \ll 1$, the magnification of the non-critical images can be approximated by $A_{\text{other}}(t) \simeq a_{\text{other}} [1 + \omega(t - t_f)]$ where a_{other} is the magnification at the caustic exit at time t_f and ω measures its variation.

As the period during which our generic fold-caustic model is believed to be a fair approximation, we choose the range $2463.45 \leq \text{HJD} - 2450000 \leq 2467$. Restricting our attention to those data sets with more than two points in this region leaves us with 29 points from SAAO and 15 points from UTas in I as well as 98 points from the ESO 2.2m in R, amounting to a total of 142 data points. From a binary lens model of the complete data sets (Kubas et al. 2004) for these observatories and filters, we have determined the source magnitudes $m_S^{(s)}$ and the blend ratios $g^{(s)}$. With the adopted synthetic spectra, we compute the stellar intensity profiles for I and R, and use these for obtaining a fit of the generic fold-caustic model to the data in the caustic-crossing region by means of χ^2 -minimization, which determined the 5 model parameters t_f , Δt , a_{crit} , a_{other} ,

Table 1. Model parameters of a fit to data obtained by PLANET with the SAAO 1.0m, UTas 1.0m, and ESO 2.2m. on the microlensing event OGLE 2002-BLG-069. While source magnitudes $m_S^{(s)}$ and blend ratios $g^{(s)}$ result from a fit involving a binary lens model to the complete data sets, the remaining parameters have been determined by applying a generic fold-caustic model with PHOENIX limb darkening solely to the data taken around the caustic exit.

Parameter	Value	Parameter	Value
$m_S^{\text{SAAO [I]}}$	16.05	t_f (days)	2465.637
$m_S^{\text{UTas [I]}}$	16.05	Δt (days)	0.7297
$m_S^{\text{ESO 2.2m [R]}}$	16.3	a_{crit}	19.60
$g^{\text{SAAO [I]}}$	0.16	a_{other}	7.011
$g^{\text{UTas [I]}}$	0.064	ω (days) $^{-1}$	-0.04519
$g^{\text{ESO 2.2m [R]}}$	0.0083		

and ω as shown in Tab. 1. If a classical linear limb darkening is included in the list of parameters to fit (as in Albrow et al. 1999b), the best fit is obtained with $\Gamma = 0.5$.

The modeled light curve and the structure of the residuals of the two fits are given in the lower panels of Fig. 1. The fit with adopted PHOENIX limb darkenings clearly show systematic trends at the level of 1-2 %. The same trends in the residuals can be seen from the figure, which suggests some specific features lying in the real stellar atmosphere. We checked whether this discrepancy can be caused by the straight fold caustic approximation, but from running the already mentioned global binary lens model neither the very small curvature of the caustic nor the source trajectory can explain this systematic effect.

4. Comparison between synthetic spectra and spectroscopic data

The fold-caustic model derived in Sec. 3 is used to compute the source flux during the caustic exit in order to obtain a synthetic spectrum at each epoch in a consistent way. In Fig. 2 we show the observed and synthetic spectra at two epochs: 9 July at UT 00h04 and 9 July at UT 22h59 (trailing limb crossing the caustic). A first analysis reveals good agreement between UVES and synthetic spectra for the wings part of H α (6558 – 6561.8 Å and 6563.8 – 6567.6 Å), whereas a clear discrepancy is observed in its core (6561.8 – 6563.8 Å). We note that the chromosphere is not included in the PHOENIX calculations. Although it should have a minor influence on the broadband limb darkenings, it will have an effect on the core of lines like H α . We therefore divided the analysis in two parts: the wings and the core. In order to compare the observed equivalent widths of the H α -line with the predictions from our synthetic spectrum, we apply an overall scale factor to the equivalent width (1.035 for the wings part and 1.495 for the core part of the line), so that the measurements derived from the fiducial model match the post-caustic observations.

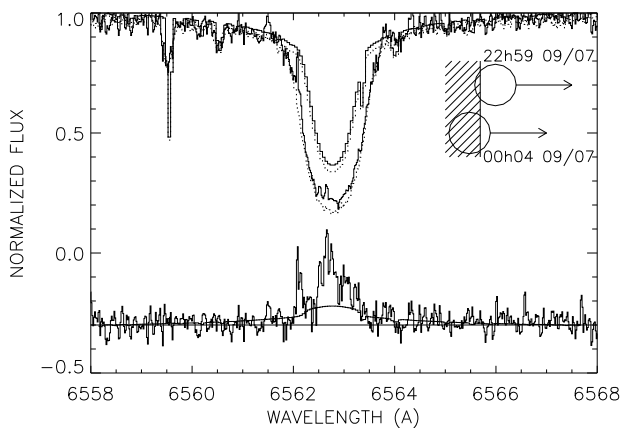


Fig. 2. Upper panel: two UVES spectra (two lower curves) corresponding to 9 July, UT 22h59 (HJD – 2450000 = 2465.47, solid line) and 9 July at UT 00h04 (reference spectra, HJD – 2450000 = 2464.51, dotted line), as well as two computed synthetic spectra at the same epochs (the two upper solid and dotted curves). Lower panel: fractional difference $\delta F^\lambda = 2(F_{00h04}^\lambda - F_{22h59}^\lambda)/(F_{00h04}^\lambda + F_{22h59}^\lambda)$ (lower solid line) for wavelengths in the vicinity of the $H\alpha$ -line shifted vertically by -0.3 . Both the observations and the model are shown. On the upper right, we show the relative position of the source star at each epoch with respect to the fold-caustic shown as dashed.

The observed and predicted temporal variations of the equivalent widths of both the wings and the core of $H\alpha$ are plotted in the upper part of Fig. 1. Note at the beginning a small short-term decrease in the model, when the leading limb hits the caustic, followed by little variation while the source centre crosses, but then a marked change when the trailing limb exits the caustic. The spectral profile of the core is not well matched by the model spectrum as seen in Fig. 2; both the width and the depth disagree. Furthermore, the differential variation in flux between the centre and the limb is not well reproduced, even after the scale factor has been applied. A better fit is obtained to the wings. Both parts of the line show larger equivalent width variations than predicted by the model.

Last but not least, in the spectrum corresponding to 10 July, UT 02h58 shown in Fig. 3, we clearly note a strong deviation in the core of the line but a much smaller one in the wing. For the purpose of the following discussion, we define the effective photospheric radius of the star as that at which the R band intensity has fallen to 5 % of the central intensity in R. Using the fit done with limb darkening derived from PHOENIX model, we infer that the spectrum started when the caustic was at a fractional radius $\rho = 0.996$ and ended at $\rho = 1.015$ while with a linear limb-darkening law, the spectrum started at a fractional radius $\rho = 1.007$ and ended at $\rho = 1.026$.

In both cases, it is clear that the spectrum was taken when the caustic was outside the photosphere in R. There is a clear emission peak in the core of the $H\alpha$ absorption line, and this can only exist provided there is a temperature inversion in the atmosphere (i.e. a chromosphere). The doppler shift of the emission core is consistent with material moving outward through the giant source star’s chromosphere ($H\alpha$ emission

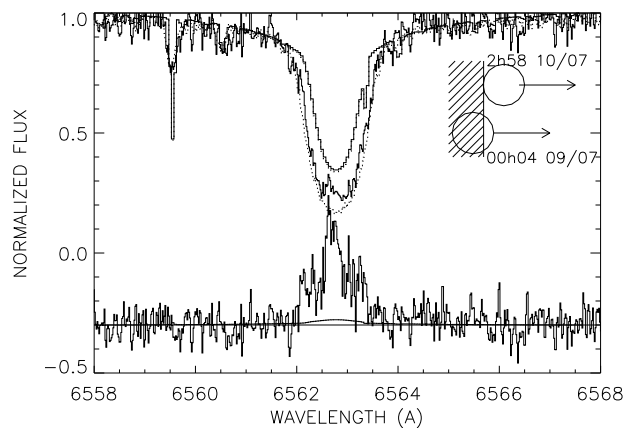


Fig. 3. Same Legend as Fig. 2 but for the pair of spectra 9 July at UT 00h04. and 10 July, UT 02h58. Notice the strong signature of the chromospheric $H\alpha$ emission.

line) with a radial velocity of $\approx 7 \text{ kms}^{-1}$, the signature being amplified at the very end of the caustic exit.

Acknowledgements. For this particular VLT follow up exercise, we are expressing our highest gratitude to the ESO staff at Paranal and La Silla whose flexibility and efficiency was absolutely vital to the success of the observations. We are very grateful to OGLE-III for their Early Warning System (EWS), to the observatories that support our science (European Southern Observatory, Canopus, CTIO, Perth, SAAO) via the generous allocations of time that make this work possible. We thank Andy Gould and Dimitar Sasselov for fruitful discussions. The operation of Canopus Observatory is in part supported by the financial contribution from David Warren, and the Danish telescope at La Silla is operated by IJAF financed by SNF. JPB acknowledges financial support via award of the “Action Thématique Innovante” INSU/CNRS. MD acknowledges postdoctoral support on the PPARC rolling grant PPA/G/O/2001/00475.

References

- Abe, F., Bennett, D., Bond, I., et al. 2003, *A&A*, 411, L493
 Afonso, C., Albert, J., Andersen, J., et al. 2001, *A&A*, 378, 1014
 Albrow, M.D. Beaulieu, J., Caldwell, J., et al. 1999a, *ApJ*, 522, 1022
 —. 1999b, *ApJ*, 522, 1011
 —. 2001, *ApJ*, 550, L173
 Allard, F., Hauschildt, P., Alexander, D., Tamanai, A., & Schweitzer, A. 2001, *ApJ*, 556, 357
 Beaulieu, J. P., Brilliant, S., Cassan, A., et al. 2004, in preparation
 Bryce, H., Hendry, M., & Valls-Gabaud, D. 2002, *A&A*, 388, L1
 Castro, S., Pogge, R., Rich, M., Depoy, D., & Gould, A. 2001, *ApJ*, 548, L197
 Claret, A. & Hauschildt, P. H. 2003, *A&A*, 412, 241
 Fields, D. L., Albrow, M. D., An, J., et al. 2003, *ApJ*, 596, 1305
 Heyrovský, D., Sasselov, D., & Loeb, A. 2000, *ApJ*, 543, 406
 Jørgensen, U., Carlsson, M., & Johnson, H. 1992, *A&A*, 254, 258
 Kubas, D., Cassan, A., Beaulieu, J., et al. 2004, in preparation

- Loeb, A. & Sasselov, D. 1995, ApJ, 449, L33
Minniti, D., Barbuy, B., Hill, V., et al. 2002, A&A, 384, 884
Orosz, J. A. & Hauschildt, P. H. 2000, A&A, 364, 265
Schneider, P. & Wagoner, R. V. 1987, ApJ, 314, 154
Udalski, A. 2003, Acta Astronomica, 53, 291